



Dynamical system analysis of quantum tunneling in an asymmetric double-well potential

Swetamber Das ^{a)} and Arghya Dutta ^{b)}

Department of Physics, SRM University-AP, Amaravati 522240, Andhra Pradesh, India

We study quantum tunneling in an asymmetric double-well potential using a dynamical systems-based approach rooted in the Ehrenfest formalism. In this framework, the time evolution of a Gaussian wave packet is governed by a hierarchy of coupled equations linking lower- and higher-order position moments. An approximate closure, required to render the system tractable, yields a reduced dynamical system for the mean and variance, with skewness entering explicitly due to the potential's asymmetry. Stability analysis of this system identifies energy thresholds for detectable tunneling across the barrier and reveals regimes where tunneling, though theoretically allowed, remains practically undetectable. Comparison with full numerical solutions of the time-dependent Schrödinger equation shows that, beyond reproducing key tunneling features, the dynamical systems approach provides an interpretable description of quantum transport through tunneling in an effective asymmetric two-level system.

^{a)}Electronic mail: swetamber.p@srmap.edu.in

^{b)}Electronic mail: arghya.d@srmap.edu.in

I. INTRODUCTION

Quantum mechanical tunneling in double-well potentials remains a central framework for probing the dynamics of two-level quantum systems^{1–3}. From microscopic processes such as the inversion of the ammonia molecule⁴ and electron tunneling in two coupled quantum dots⁵ to macroscopic processes including tunneling in Bose–Einstein condensates^{6–9} and in superconducting quantum interference devices^{10–13}, a wide range of physical and chemical systems can be studied within such an effective two-level description. Remarkably, despite the complexities of macroscopic tunneling involving many particles, the dynamics of such systems can often be modeled with reasonable accuracy as a single particle moving and tunneling in an effective double-well potential $\phi(x)$ defined over some collective macroscopic coordinate x ¹⁴.

However, studying the full quantum dynamics of even a simplified single-particle system becomes challenging when the potential cannot be treated perturbatively, thereby falling outside the scope of Fermi’s golden rule¹⁵. In such cases—for instance tunneling in double-well potentials—the semiclassical Wentzel–Kramers–Brillouin (WKB) approximation has been widely employed, often together with the simplifying assumption that the two wells can be modeled as simple harmonic oscillator potentials^{3,14,16–18}. Despite its broad utility, the WKB approach faces some limitations.

A central restriction of the WKB approximation arises from its validity condition, which requires the particle momentum $p(x) = \sqrt{2m|E - \phi(x)|}$ to remain sufficiently large. This assumption breaks down near classical turning points, where the momentum vanishes, and within potential wells for low-energy states, particularly the ground state, where both kinetic and potential energies may become small³. Further, especially near the boundaries where wave functions must be matched across classically allowed and forbidden regions, the standard WKB wavefunctions often require fine-tuning¹⁹.

In addition, traditionally, the WKB approach has been mainly employed to obtain approximate solutions of the *time-independent* Schrödinger equation. By contrast, time-dependent WKB and other such semiclassical methods remain an active area of research^{20–24}. This limitation becomes particularly significant when studying tunneling—an inherently time-dependent quantum phenomenon²⁵. For instance, in a double-well potential, tunneling is theoretically permitted at all sub-barrier energies. However, tunneling becomes practically undetectable for states deep within the wells since it is exponentially suppressed. This poses a significant impediment in studying systems like ultracold optical lattices²⁶, where such suppression prohibits the detection of small tunnel splittings²⁷. Overcoming this challenge to predict a practical quantitative energy threshold for detectable quantum transport through tunneling requires a theoretical framework capable of modeling time-dependent quantum evolution directly, a task for which the standard time-dependent WKB approximation is ill-suited.

To bridge this gap, we turn to alternative complementary theoretical frameworks that naturally connect classical and quantum dynamics. Among them, a systematic approach is provided by the Ehrenfest theorem^{28–30}, which, although often introduced as a means to extract the semiclassical limit, yields exact quantum mechanical equations governing the time evolution of expectation values of operators, and is therefore not limited to describing the classical limit of quantum mechanics^{31–35}. For a quantum operator \mathcal{O} that does not depend explicitly on time, the time evolution of its expectation value in a system described

by a Hamiltonian H is given by the Ehrenfest theorem:

$$\frac{d}{dt}\langle\mathcal{O}\rangle = \frac{1}{i\hbar}\langle[\mathcal{O}, H]\rangle, \quad (1)$$

which is fundamentally equivalent to the Heisenberg equation of motion for operators and provides a general framework for extracting quantum dynamics directly from the evolution of expectation values.

Recently, the Ehrenfest formalism has been employed to model tunneling dynamics in symmetric double-well^{36,37} and Morse³⁸ potentials, treating them as effective dynamical systems. For a single particle initially described by a Gaussian wave packet, Eq. 1 enables the reconstruction of the full time evolution of the system through the dynamics of its moments $\langle x^n \rangle$, where n denotes the order of the moment. While for Hamiltonians containing terms beyond quadratic order, the lower-order moment equations couple to higher-order ones, necessitating approximate closures^{39,40}, this formalism naturally highlights the distinction between classical and quantum dynamics, since the presence of uncertainty relations among non-commuting observables makes the quantum moments evolve very differently from their classical counterparts^{40–44}.

Here we employ the dynamical systems approach to study quantum tunneling of a particle, represented by a Gaussian wave packet, in a one-dimensional asymmetric double-well potential. Such asymmetry breaks the system's reflection symmetry, inducing highly directional tunneling important in several physical processes, including tunneling in strong-field ionization⁴⁵ and proton transfer in photosynthesis⁴⁶. Through a stability analysis of the four-dimensional dynamical system governing the wave packet's mean and variance, we compute a practical estimate of the energy threshold required for a detectable signature of tunneling across the barrier between the two wells. This threshold is determined by the skewness of the wave packet's position distribution, which quantifies the potential's asymmetry. Consequently, we incorporate skewness as a key ingredient in our analysis to determine the energy range above which detectable tunneling occurs, indicated by switching of the mean position $\langle x \rangle$ between the two wells as the system evolves. Comparison with numerical solutions to the full time-dependent Schrödinger demonstrates that the reduced dynamical model reliably captures the essential features of asymmetric tunneling dynamics, while offering additional insight on practical tunneling energy thresholds.

II. METHOD

A. Double-well potentials

We begin with a brief discussion on the double-well potentials which can be represented by

$$\phi(x) = \frac{a}{2}x^2 - \frac{b}{3}x^3 + \frac{c}{4}x^4, \quad (2)$$

where a , b , and c are positive parameters. Depending on the choice of these parameters, Eq. 2 can represent either a symmetric or an asymmetric double-well potential.

The three stationary points of the potential are obtained by solving $\phi'(x) = 0$, which gives $x = 0$ and $x = \beta_{\pm}$ where $\beta_{\pm} \equiv (b \pm \sqrt{b^2 - 4ac})/2c$. The solutions β_{\pm} are real only if

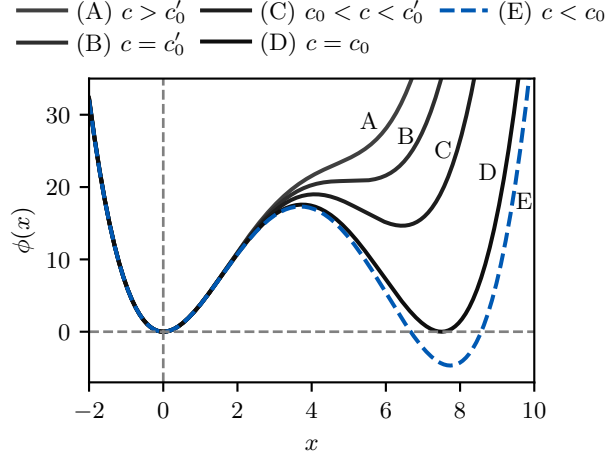


FIG. 1. **Symmetric and asymmetric double-well potentials.** Representative forms of the quartic potential $\phi(x)$ (Eq. 2) are shown with fixed $a = 10$ and $b = 4$, and varying c . Curves A–E illustrate the transition from a single well to symmetric and asymmetric double-well configurations, respectively, as c decreases. The asymmetric double-well potential with $c = 0.35$ (curve E, blue, dashed) is studied in this work.

the discriminant is non-negative, or equivalently $c \leq c'_0 \equiv b^2/4a$. The two stationary points at β_{\pm} coalesce for $c = c'_0$, giving a single stationary point $\beta \equiv b/2c$. Evaluating $\phi''(x)$ at the stationary point $x = 0$ reveals $\phi''(0) = a$, showing that $x = 0$ is a local maximum if $a < 0$ and is a local minimum if $a > 0$. Throughout this work, we will take $a > 0$.

At $c = c'_0$, the stationary point at $x = \beta \equiv b/2c$ satisfies $\phi''(\beta) = 0$ (and $\phi'''(\beta) = b \neq 0$), corresponding to the appearance of an inflection point. For $c > c'_0$, the potential has only one minimum at $x = 0$.

To obtain a symmetric double well, we additionally require $\phi(x) = 0$ to have nontrivial roots. Solving for $\phi(x) = 0$ yields $x = 0$ and $x = \alpha_{\pm}$ where $\alpha_{\pm} = 2b/3c \pm (2/c)\sqrt{b^2/9 - ac/2}$. When $c > c_0 \equiv 2b^2/9a$, $x = 0$ is the only real root. At $c = c_0$, the two roots α_{\pm} merge to a single value $\alpha \equiv 2b/3c = 3a/b$ (since $c = 2b^2/9a$), where $\phi'(\alpha) = 0$ and $\phi''(\alpha) = a$, giving a minimum of the potential since we took $a > 0$ for this paper. Again notice that the non-zero roots of $\phi'(x) = 0$ at $c = c_0 \equiv 2b^2/9a$ take the values $\beta_+ = 3a/b = \alpha$, corresponding to the second well at finite x , and $\beta_- = 3a/2b$, corresponding to the potential hill located between the two minima.

Figure 1 summarizes the discussion. For positive fixed values of a and b , the potential has a single minimum at $x = 0$ when $c > c'_0 (\equiv b^2/4a)$ (curve A). An inflection point appears when $c = c'_0$ (curve B). For $c_0 < c < c'_0$ with $c_0 \equiv 2b^2/9a$, the potential contains a global minimum at $x = 0$ and a local minimum at $x = \beta_+$ (curve C), separated by a barrier at $x = \beta_-$. At $c = c_0$, the two minima become degenerate, yielding a symmetric double well (curve D). Finally, for $c < c_0$, the global minimum shifts to $x = \beta_+$, where $\phi(\beta_+) < \phi(0) = 0$, giving an asymmetric double well (curve E). In this paper, we focus on the asymmetric double-well potential described by curve E.

B. Dynamical equations

Consider a particle of mass $m = 1$ moving in the asymmetric double-well potential described by Eq. 2. The Hamiltonian of the system is

$$H = \frac{p^2}{2} + \phi(x) = \frac{p^2}{2} + \frac{a}{2}x^2 - \frac{b}{3}x^3 + \frac{c}{4}x^4. \quad (3)$$

To construct the dynamical system comprising time evolutions of the mean position $\langle x \rangle$ and the variance $V \equiv \langle x^2 \rangle - \langle x \rangle^2$ of the particle, we employ the Ehrenfest theorem (Eq. 1) and simplify the commutators to obtain

$$\frac{d\langle x \rangle}{dt} = \langle p \rangle, \quad (4)$$

$$\begin{aligned} \frac{d^2\langle x \rangle}{dt^2} &= -\langle \phi' \rangle \\ &= -a\langle x \rangle + b[V + \langle x \rangle^2] - c[S + 3V\langle x \rangle + \langle x \rangle^3], \end{aligned} \quad (5)$$

$$\frac{dV}{dt} = \langle xp + px \rangle - 2\langle x \rangle \langle p \rangle, \quad (6)$$

$$\begin{aligned} \frac{d^2V}{dt^2} &= 2V_p - 2(\langle x\phi' \rangle - \langle x \rangle \langle \phi' \rangle) \\ &= 4E - 2\langle p \rangle^2 - a[4V + 2\langle x \rangle^2] + b\left[\frac{10}{3}S + 8V\langle x \rangle + \frac{4}{3}\langle x \rangle^3\right] \\ &\quad - c[9V^2 + 10S\langle x \rangle + 12V\langle x \rangle^2 + \langle x \rangle^4]. \end{aligned} \quad (7)$$

In Eq. 7, $V_p \equiv \langle p^2 \rangle - \langle p \rangle^2$ is the variance of the particle's momentum. It is related to the total energy of the system $E(\equiv \langle H \rangle)$ since $\langle p^2 \rangle = 2E - 2\langle \phi \rangle$. The mean energy E is the only conserved quantity of this system, serving as a control parameter for the dynamics. In Eqs. 5 and 7, $S \equiv \langle (x - \langle x \rangle)^3 \rangle$ is the skewness and $K \equiv \langle (x - \langle x \rangle)^4 \rangle$ is the kurtosis, which we simplified with the Gaussian approximation $K = 3V^2$. This approximation is reasonable because we represent the unit-mass particle as a Gaussian wave packet

$$\psi(x, t) = \frac{1}{\sqrt[4]{2\pi V}} \exp\left[-\frac{(x - \langle x \rangle)^2}{4V} + ik(x - \langle x \rangle)\right], \quad (8)$$

where k is the wave number, and expect its shape to retain the properties of a Gaussian distribution, to a large extent. Notice that both the variance and the mean position of this wave packet depend on time.

If we start with a Gaussian wave packet initialized at $\langle x \rangle(0) = 0$, variance $V(0) = V_0$, and wave number $k(0) = k_0$ at time $t = 0$, computing the expectation value of the Hamiltonian (Eq. 3) in this wave packet provides a connection between the conserved total energy E and the initial variance V_0 :

$$E = \frac{1}{8V_0} + \frac{k_0^2}{2} + \frac{a}{2}V_0 + \frac{3}{4}cV_0^2, \quad (9)$$

where we have set $\hbar = 1$. With these definitions, we now proceed to analyze the four-dimensional dynamical system.

III. RESULTS AND DISCUSSIONS

A. Stability analysis

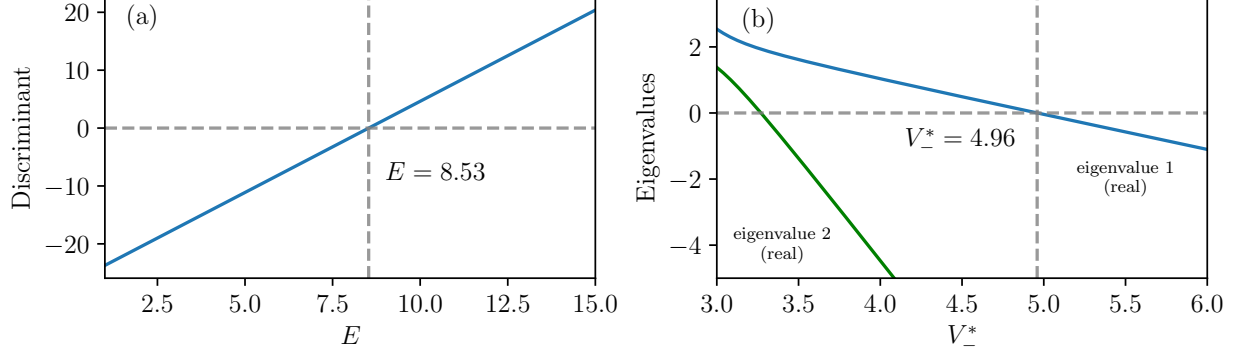


FIG. 2. **Stability analysis.** (a) The solutions for V_* of the quadratic equation (Eq. 13) are real only when the discriminant is non-negative. This condition is satisfied for energies $E \geq 8.53$, which is the minimum energy needed for the existence of the fixed point V_* . (b) The real parts of the two eigenvalues of the stability matrix for the fixed point $(\beta_-, 0, V_*, 0)$, associated with the potential hill, are plotted against V_* . Both eigenvalues are negative beyond $V_* = 4.96$, corresponding to $E = 10.60$. This signifies the transition of the potential hill from a classically unstable fixed point to a stable one, indicating the onset of tunneling.

To analyze the stability of the four-dimensional dynamical system described by Eqs. 4–7, we first linearize them as follows:

$$\frac{d^2}{dt^2} \begin{pmatrix} \delta \langle x \rangle \\ \delta V \end{pmatrix} = \mathbf{A} \begin{pmatrix} \delta \langle x \rangle \\ \delta V \end{pmatrix}, \quad (10)$$

where the stability matrix \mathbf{A} is given by:

$$\mathbf{A} = \begin{pmatrix} (-a + 2b\langle x \rangle - 3c\langle x \rangle^2 - 3cV) & (b - 3c\langle x \rangle) \\ (-4a\langle x \rangle + 4b\langle x \rangle^2 - 4c\langle x \rangle^3 + 8bV - 24c\langle x \rangle V - 10cS) & (-4a + 8b\langle x \rangle - 18cV - 12c\langle x \rangle^2) \end{pmatrix}. \quad (11)$$

The fixed points of the system are of the form $(\langle x \rangle^*, 0, V^*, 0)$. For such a fixed point to exist, skewness S must be set by V^* . The constant value of skewness at the fixed point is a consequence of reducing the dynamical system to four dimensions involving mean and variance. We find the relation between them by equating Eq. 5 to zero (and since $c \neq 0$):

$$S = -\frac{1}{c} [a\langle x \rangle^* - bV^* - b\langle x \rangle^{*2} + 3cV^*\langle x \rangle^* + c\langle x \rangle^{*3}]. \quad (12)$$

We substitute this expression for S in Eq. 7 to obtain an equation for V^* :

$$\begin{aligned} \frac{9c}{4}V^{*2} + \left(a - \frac{5b^2}{6c} + 3b\langle x \rangle^* - \frac{9c\langle x \rangle^{*2}}{2}\right)V^* + \\ \left[\frac{5ab\langle x \rangle^*}{6c} - 2a\langle x \rangle^{*2} - \frac{5b^2\langle x \rangle^{*2}}{6c} + 3b\langle x \rangle^{*3} - \frac{9c\langle x \rangle^{*4}}{4}\right] = E. \end{aligned} \quad (13)$$

This quadratic equation can be solved numerically for given values of $\langle x \rangle^*$ and energy E . Real solutions for V^* exist only when the discriminant of Eq. 13 is non-negative.

Next, we analyze the existence and stability of the three fixed points given by (a) $(0, 0, 0, V_0^*)$, (b) $(\beta_-, 0, V_-^*, 0)$, and (c) $(\beta_+, 0, V_+^*, 0)$. The fixed points (a) and (c) correspond to the two minima and (b) indicates the local maxima of the potential. As mentioned in Fig. 1, the parameters of the asymmetric double-well potential (Eq. 2) used in this study are $a = 10$, $b = 4$, and $c = 0.35$.

We first consider the case of the local maxima at $x = \beta_- = (b - \sqrt{b^2 - 4ac})/2c$, which is about 3.69 for the chosen parameter values and numerically analyze its stability. The discriminant from Eq. 13 versus energy is plotted in Fig. 2(a), and it shows that real solutions exist when $E \geq 8.53$. Stability analysis further shows that the fixed point $(\beta_-, 0, V_-^*, 0)$ becomes stable when the real parts of both eigenvalues of the matrix \mathbf{A} (Eq. 11) are negative. We compute and plot them in Fig. 2(b) which shows that both are negative for $V_-^* \geq 4.96$. This value of V_-^* corresponds to $E = 10.60$ from Eq. 13. This is the energy threshold above which we expect tunneling to occur. We now list our findings below:

1. Real solutions for V_-^* do not exist when $E < 8.53$. There are no fixed points below this energy threshold.
2. In the regime $8.53 \leq E < 10.60$, the fixed point exists, but it is unstable and tunneling does not occur.
3. For $10.60 \leq E < 17.31$, the classically unstable fixed point at the potential hill top becomes stable and tunneling takes place.
4. Energies higher than $E = 17.31$ are irrelevant for tunneling because they exceed the barrier height.

In case of the two potential minima, the corresponding fixed points (a) and (c) always exist for any positive value of E and both are stable. To see this, we first consider the fixed point (a) for which $\langle x \rangle^* = 0$. This yields the following condition for real solution of V_0^* to exist: $E \geq -(a - 5b^2/6c)^2/9c$. Because $c > 0$, the lower bound on the inequality is trivially satisfied as E must be non-negative. The other fixed point (c) $(\beta_+, 0, V_+^*, 0)$ is located at the global minima on the right at $x = \beta_+ = 7.73$. Like the fixed point (a), we get a real solution for V_+^* for any positive value of energy. The two fixed points (a) and (c) are therefore irrelevant for the tunneling dynamics.

B. Numerical Results: Dynamical systems approach

Assuming the fixed point $(\beta_-, 0, V_-^*, 0)$ exists at the local maximum at $x = \beta_- = 3.69$, we solve the system of Eqs. 4–7. The skewness S in these equations is calculated from Eq. 12

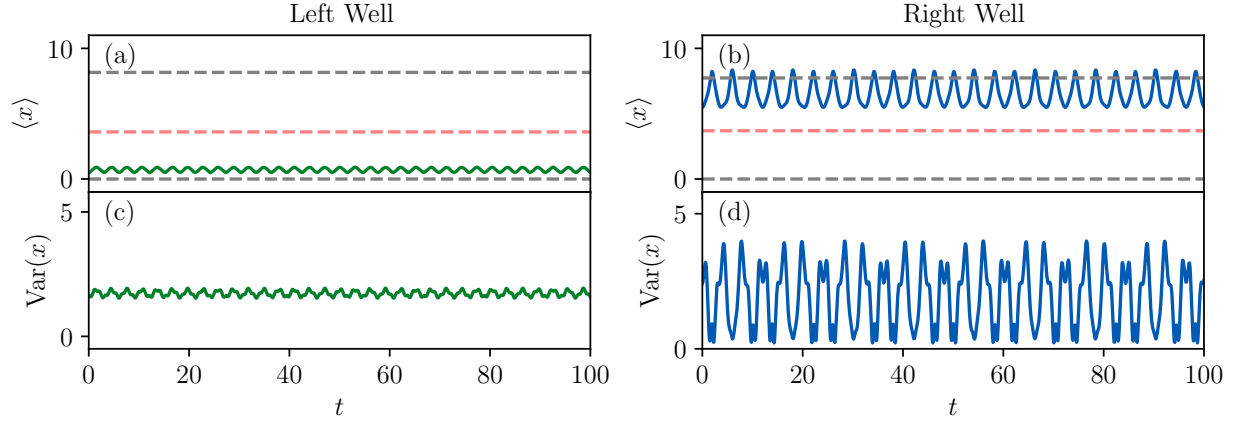


FIG. 3. **No tunneling (dynamical systems analysis).** The time evolution of the mean position $\langle x \rangle$ of the wave packet is shown for initializations in (a) the left well ($\langle x \rangle(0) = 0.5$, $E = 9.0$) and (b) the right well ($\langle x \rangle(0) = 5.50$, $E = \Delta + 9.0$, where $\Delta = 4.68$ is the energy difference between the two minima). In both cases, $\langle x \rangle$ oscillates but remains confined within its well. The red dashed line at $\langle x \rangle = 3.69$ indicates the maxima at the potential hill, and the gray dashed line at $\langle x \rangle = 0$ and 7.73 mark the potential minima for the left and right wells, respectively. The variance in the right well (panel (d)) is larger than in the left well (panel (c)). This difference can be attributed to the higher energy ($E = \Delta + 9.0$) of the wave packet in the right well compared to the left well ($E = 9.0$).

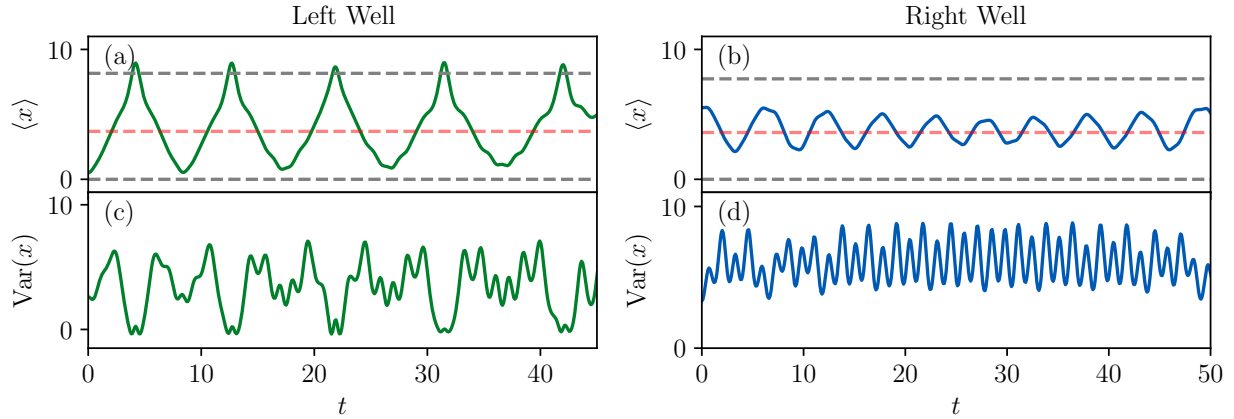


FIG. 4. **Tunneling (dynamical systems analysis).** The time evolution of the mean position $\langle x \rangle$ of the wave packet is shown for initializations in (a) the left well ($\langle x \rangle(0) = 0.5$, $E = 14.95$) and (b) the right well ($\langle x \rangle(0) = 5.50$, $E = \Delta + 14.95$, where $\Delta = 4.68$ is the energy difference between the two minima). In panels (a) and (b), $\langle x \rangle$ switches between the two wells—indicating detectable tunneling. The red dashed line at $\langle x \rangle = 3.69$ indicates the maxima at the potential hill, and the gray dashed line at $\langle x \rangle = 0$ and 7.73 mark the potential minima for the left and right wells, respectively. The variance in the right well (panel (d)) is larger than in the left well (panel (c)), owing to the higher total energy. Interestingly, the variance in the right well oscillates rapidly, along with frequent barrier crossings, compared to the left well where the particle makes longer excursions between the wells.

for this fixed point. The initial conditions are chosen such that both the initial variance $V(0) = V_0$ and its time derivative $dV/dt|_{t=0}$ are zero.

We investigate the system's tunneling behavior below the energy threshold. The system is initialized within the left well at $\langle x \rangle(0) = 0.5$ with an energy $E = 9.0$, which is below the tunneling threshold of 10.60. These total energy and the initial wave vector k_0 (or equivalently the momentum p_0) determine the initial variance $V(0)$ of the wave packet via Eq. 9, allowing the dynamical equations to be numerically integrated. We set k_0 to zero throughout this work. The resulting time series for the mean position $\langle x \rangle$ (green curve, Fig. 3(a)) shows oscillations confined to the left well. In all subsequent $\langle x \rangle$ time series plots, red dashed line marks the local maxima (barrier top), and gray dashed lines mark the left and the right potential minima.

Similarly, when initialized in the right well with $\langle x \rangle(0) = 5.5$ (blue curve, Fig. 3(b)), the particle remains localized. In both cases, the absence of switching between the wells confirms that tunneling does not occur. This localization is corroborated by the time evolution of the variance $V(t)$ which remains low, indicating no barrier crossings (Fig. 3(c) and (d)). Interestingly, fluctuations are smaller in the shallower left well than in the deeper right well. The larger fluctuations around the mean position in the right well suggest that tunneling is impending at this energy but has not yet been triggered.

At an energy of $E = 14.95$, which exceeds the tunneling threshold, we observe clear tunneling from the left to the right well. This is evidenced by the time series of $\langle x \rangle$ (green curve, Fig. 4(a)), which exhibits large-amplitude oscillations that frequently cross the potential barrier, indicating switching between wells. To observe the reverse process, i.e. tunneling from the right to the left well, the system requires additional energy equal to the energy difference between the two wells $\Delta = 4.68$. When initialized in the right well at a higher energy $E = 14.95 + \Delta$, the mean position (blue curve, Fig. 4(b)) shows similar switching dynamics, confirming continuous bi-directional tunneling. The mean variance during the left-to-right tunneling (Fig. 4(c), green curve) is smaller than its value during right-to-left tunneling (Fig. 4(d), blue curve). Interestingly, when initiated in the right well, the wave packet keeps switching rapidly across the barrier, but when initiated in the left well, it makes more sustained excursions into both wells, spending less time near the barrier.

C. Numerical Results: Schrödinger Equation solution

We now compare the dynamical systems-based approach discussed in the previous section with a high-fidelity numerical solution of the time-dependent Schrödinger equation. The numerical integration is performed using the Crank–Nicolson method⁴⁷, chosen for its unconditional stability and property of unitary evolution, which keeps the wave function's norm and system's total energy nearly constant. To achieve high accuracy, we confine the particle in a box ($x \in [-100, 100]$) and then discretize it into a grid of $N = 10^5$ points ($\Delta x = 0.002$), while using a small time step of $\Delta t = 0.01$. Dirichlet boundary conditions ($\psi(x_{\min}) = \psi(x_{\max}) = 0$) are enforced at each time step. The large box size, compared to the separations between the potential extrema, ensures the reflecting boundaries are located far from the region of interest, preventing any spurious reflections from affecting the dynamics over the simulation time. This implementation ensures that the drift in both the norm and total energy remains below 10^{-10} throughout the simulation time.

As before, the energy separation between the two minima is given by $\Delta = 4.68$. Because of exponential suppression of the wave packet across the potential barrier, we find that

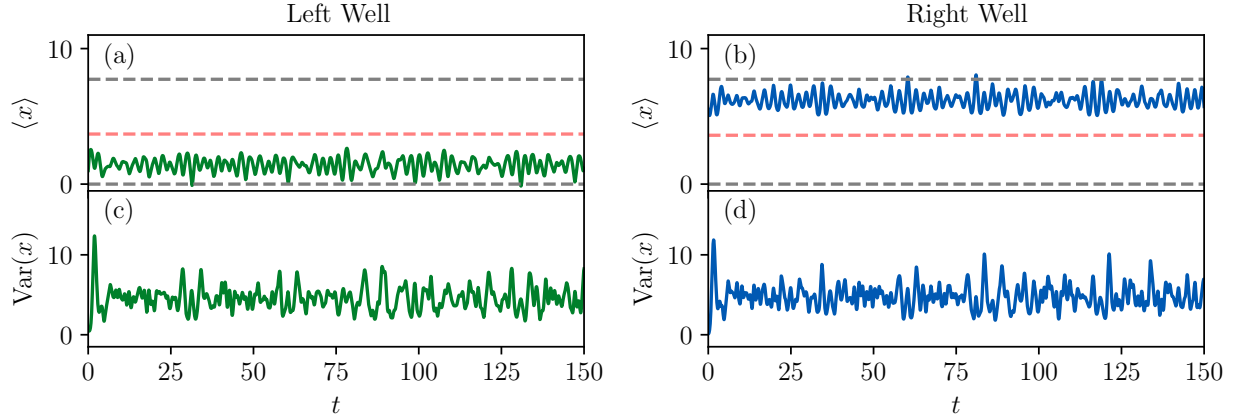


FIG. 5. **No tunneling (Full Schrödinger simulation).** Time evolution of mean position $\langle x \rangle$ of the wave packet initialized at (a) $\langle x \rangle(0) = 0.5$ with $E = 9.0$ in the left well and (b) at $\langle x \rangle(0) = 5.50$ with $E = \Delta + 9.0$ in the the right well, where $\Delta = 4.68$ is the depth of the right well relative to the left. The wave packet oscillates but does not cross the barrier. The red dashed line ($\langle x \rangle = 3.69$) indicates the potential hill top. The gray dashed lines at $\langle x \rangle = 0$ and 7.73 indicate the location of potential minima in the left and right wells, respectively. The curves in panels (c) and (d) show time evolution of the variance in the left and right wells, respectively. While the mean positions are confined to their respective wells, the magnitudes and temporal fluctuations of the variance are similar.

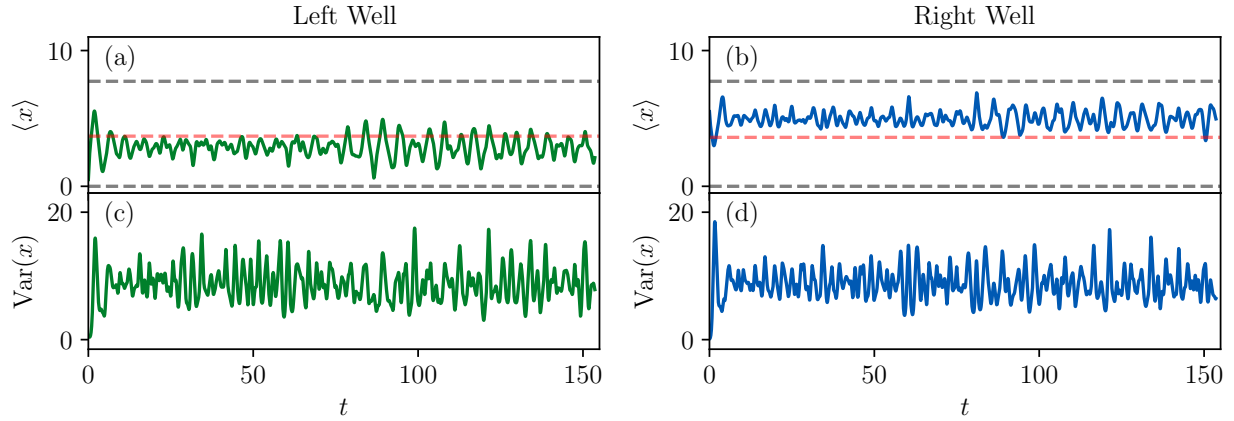


FIG. 6. **Tunneling (Full Schrödinger simulation).** Time evolution of mean position $\langle x \rangle$ of the wave packet initialized at (a) $\langle x \rangle(0) = 0.5$ with $E = 14.95$ in the left well and (b) at $\langle x \rangle(0) = 5.50$ with $E = \Delta + 14.95$ in the the right well, where $\Delta = 4.68$ is the depth of the right well relative to the left. The red dashed line ($\langle x \rangle = 3.69$) indicates the potential hill top. The gray dashed lines at $\langle x \rangle = 0$ and 7.73 indicate the location of potential minima in the left and right wells, respectively. In both panels (a) and (b), the mean position oscillates and frequently crosses the barrier—indicating detectable tunneling. The curves in panels (c) and (d) show time evolution of the variance in the left and right wells, respectively. The variance both cases are similar because, despite the significant change in $\langle x \rangle$ as it crosses the potential barrier, the time series of $\langle x \rangle$ for the two wells are only slightly shifted from one another.

detectable tunneling only occurs at energies sufficiently above Δ , within the finite times of our simulations. Especially for detecting tunneling from the right to the left well, maintaining higher energies becomes crucial. Accordingly, we set the energy baseline to Δ so that we can accurately compare the left-to-right and right-to-left tunneling. Similar to the dynamical system studied before, here we continue to use $\langle x \rangle(t)$ as the primary indicator for detecting tunneling.

To ensure a close comparison with the dynamical systems analysis for the no tunneling scenario, we initialize a Gaussian wave packet at $x(0) = 0.5$ with $E = 9$ and $x(0) = 5.5$ with $E = \Delta + 9.0$ for the left and right wells, respectively. By tuning the wave packet's variance, we achieve energies that are nearly identical to those used in the dynamical systems simulations. The subsequent quantum dynamics, characterized by the time evolution of the mean position and variance, are presented in Fig. 5 (a) and (c) for the left well and Fig. 5 (b) and (d) for the right well, respectively. The mean position fluctuates rapidly but stays within its well set by the initial location, indicating no tunneling.

Next, we initialize wave packets in both wells at $x = 0.5$ and $x = 5.5$, this time with energies increased to $E = 14.95$ for the left well and $E = \Delta + 14.95$ for the right well, again by adjusting the variance. At this energy, the mean position $\langle x \rangle$ is seen to cross the barrier, indicating bi-directional tunneling from left to right (Fig. 6(a)) and from right to left (Fig. 6(b)). Although the amplitude of oscillation in $\langle x \rangle$ is smaller than in Fig. 4(a) and (b), tunneling still takes place.

Moreover, the variance for the right well is similar to that in the left well in the no-tunneling case, as shown in Figs. 5(c) and (d). This suggests that while the wave packet's mean position is determined by the well, its fluctuations and spreading dynamics are governed by similar initial conditions and total energy. For the tunneling scenario, the corresponding time evolution of the variance $V(x)$ is presented in the lower panels (c) and (d) of Fig. 6. The variances for both initializations are again similar in magnitude, though they exhibit larger fluctuations than in the non-tunneling case (Fig. 5(c) and (d)). This enhanced spreading underscores the role of total energy in governing wave packet dynamics, a feature that persists across both localized and tunneling regimes.

The quantitative differences between the tunneling observed in the dynamical systems approach and the full Schrödinger solutions are expected due to both the truncation of higher moments for closure and the use of Gaussian approximation for the kurtosis. Nevertheless, the dynamical system solution successfully reproduces the qualitative dynamics of the particle, demonstrating its utility in modeling quantum tunneling.

IV. CONCLUSION

In conclusion, this work has demonstrated that a dynamical systems approach, rooted in the Ehrenfest theorem, provides a useful framework for analyzing detectable quantum tunneling in asymmetric double-well potentials. By approximating the quantum dynamics through a four-dimensional system of equations for the first and second-order moments, the mean position $\langle x \rangle$, the variance V , and their time derivatives, we can track the system's evolution without directly solving the Schrödinger equation. Beyond the time-independent WKB approach, this time-dependent analysis also conserves the system's mean energy, which serves as a control parameter of the system, throughout the dynamics.

For tunneling in an asymmetric double-well potential, a crucial quantification of the asymmetry is provided by the third-order moment, skewness, of the wave packet. Although

we neglect fifth or higher-order moments in this analysis (with a Gaussian approximation to treat the fourth-order Kurtosis), the skewness, intrinsically set by the potential’s parameters, directly encodes its directional asymmetry. It appears explicitly in the dynamical equations, influencing the evolution of both mean position and variance.

From a dynamical systems perspective, the potential barrier corresponds to a classically unstable fixed point. Our stability analysis reveals an energy threshold beyond which it becomes stable, leading to continuous switching of the mean position $\langle x \rangle$ between the two wells. We identify this switching behavior as detectable tunneling across the potential barrier. Full numerical simulations of the time-dependent Schrödinger equation using an initial Gaussian wave packet confirm that this theoretically predicted threshold closely approximates the energy value above which detectable tunneling occurs, with small deviations attributed to the approximations inherent in our moment-truncation scheme.

In summary, the Ehrenfest theorem-based dynamical systems framework offers a robust and versatile theoretical framework for investigating bi-directional tunneling in isolated quantum systems. The present formulation can be readily extended to more complex, realistic potentials, such as multi-well structures relevant to molecular conformers and superconducting circuits. Furthermore, incorporating non-Gaussian initial states and developing refined moment-closure schemes within this framework could enable accurate analysis of anharmonic systems relevant to anharmonic vibrational spectroscopy. Together, these features highlight the dynamical systems approach as a practical and predictive tool for modeling quantum transport.

ACKNOWLEDGMENTS

The authors thank Jayanta K. Bhattacharjee for comments.

AUTHOR DECLARATIONS

Conflict of Interest

The authors have no conflicts to disclose.

Author contributions

Swetamber Das Conceptualization (equal); Formal analysis (supporting); Software (lead); Visualization (lead); Writing – original draft (equal); Writing – review and editing (equal). **Arghya Dutta**: Conceptualization (equal); Formal analysis (lead); Software (supporting); Visualization (supporting); Writing – original draft (equal); Writing – review and editing (equal).

DATA AVAILABILITY

Data sharing is not applicable to this article as no new data were created or analyzed in this study. All numerical code that support the findings of this study are openly available

at the GitHub repository: <https://github.com/Dynamics-and-Complexity-Group/quantum-dynamics>. A permanent, versioned archive is maintained on Zenodo at: [10.5281/zenodo.1745618](https://zenodo.org/record/1745618).

REFERENCES

- ¹A. J. Leggett, S. Chakravarty, A. T. Dorsey, M. P. A. Fisher, A. Garg, and W. Zwerger, *Reviews of Modern Physics* **59**, 1 (1987).
- ²M. Grifoni, *Physical Review E* **54**, R3086 (1996).
- ³S. M. H. Halataei and A. J. Leggett, *Tunnel splitting in asymmetric double well potentials: An improved wkb calculation* (2017), arXiv:1703.05758.
- ⁴J. D. Swalen and J. A. Ibers, *The Journal of Chemical Physics* **36**, 1914 (1962).
- ⁵G. Burkard, D. Loss, and D. P. DiVincenzo, *Physical Review B* **59**, 2070 (1999).
- ⁶M. Albiez, R. Gati, J. Fölling, S. Hunsmann, M. Cristiani, and M. K. Oberthaler, *Physical Review Letters* **95**, 010402 (2005).
- ⁷Y. Shin, G.-B. Jo, M. Saba, T. A. Pasquini, W. Ketterle, and D. E. Pritchard, *Physical Review Letters* **95**, 170402 (2005).
- ⁸T. Schumm, S. Hofferberth, L. M. Andersson, S. Wildermuth, S. Groth, I. Bar-Joseph, J. Schmiedmayer, and P. Krüger, *Nature Physics* **1**, 57 (2005).
- ⁹B. V. Hall, S. Whitlock, R. Anderson, P. Hannaford, and A. I. Sidorov, *Physical Review Letters* **98**, 030402 (2007).
- ¹⁰M. H. Devoret, J. M. Martinis, and J. Clarke, *Physical Review Letters* **55**, 1908 (1985).
- ¹¹Y. Makhlin, G. Schön, and A. Shnirman, *Reviews of Modern Physics* **73**, 357 (2001).
- ¹²S. Levy, E. Lahoud, I. Shomroni, and J. Steinhauer, *Nature* **449**, 579 (2007).
- ¹³J. Clarke and F. K. Wilhelm, *Nature* **453**, 1031 (2008).
- ¹⁴G. Rastelli, *Physical Review A* **86**, 012106 (2012).
- ¹⁵C. Cohen-Tannoudji, B. Diu, and F. Laloë, *Quantum mechanics. Volume 2: Angular momentum, spin, and approximation methods* (Wiley-VCH Verlag GmbH & Co. KGaA, 2020), 2nd ed., ISBN 978-3-527-34554-0, (See section C of chapter XIII).
- ¹⁶A. Garg, *American Journal of Physics* **68**, 430 (2000).
- ¹⁷D.-Y. Song, *Annals of Physics* **323**, 2991 (2008).
- ¹⁸D.-Y. Song, *Annals of Physics* **362**, 609 (2015).
- ¹⁹N. Wine, J. Achtymichuk, and F. Marsiglio, *AIP Advances* **15** (2025).
- ²⁰D. Huber and E. J. Heller, *The Journal of Chemical Physics* **87**, 5302 (1987).
- ²¹D. Huber, E. J. Heller, and R. G. Littlejohn, *The Journal of Chemical Physics* **89**, 2003 (1988).
- ²²M. Boiron and M. Lombardi, *The Journal of Chemical Physics* **108**, 3431 (1998).
- ²³Y. Goldfarb, J. Schiff, and D. J. Tannor, *The Journal of Chemical Physics* **128**, 164114 (2008).
- ²⁴C.-C. Chou and R. E. Wyatt, *The Journal of Chemical Physics* **129**, 124113 (2008).
- ²⁵C. M. Bender and D. W. Hook, *Journal of Physics A: Mathematical and Theoretical* **44**, 372001 (2011).
- ²⁶C. Gross and I. Bloch, *Science* **357**, 995 (2017).
- ²⁷L. Raso, M. Ceotto, and E. Pollak, *The Journal of Physical Chemistry Letters* **16**, 4844 (2025).
- ²⁸P. Ehrenfest, *Zeitschrift für Physik* **45**, 455 (1927).
- ²⁹E. J. Heller, *The Journal of Chemical Physics* **62**, 1544 (1975).

- ³⁰A. K. Pattanayak and W. C. Schieve, Physical Review Letters **72**, 2855 (1994).
- ³¹A. Roy and J. K. Bhattacharjee, Physics Letters A **288**, 1 (2001).
- ³²S. Biswas, R. Chattopadhyay, and J. K. Bhattacharjee, Physics Letters A **382**, 1202 (2018).
- ³³R. Chawla and J. K. Bhattacharjee, The European Physical Journal B **92**, 196 (2019).
- ³⁴P. Sarkar and J. K. Bhattacharjee, Physical Review E **102**, 052204 (2020).
- ³⁵A. Bhattacharyya, J. K. Bhattacharjee, and D. Sinha, American Journal of Physics **89**, 627 (2021).
- ³⁶S. Choi, R. Onofrio, and B. Sundaram, Physical Review E **92**, 042907 (2015).
- ³⁷S. Ray, S. Bhattacharyya, and J. K. Bhattacharjee, Physics Letters A **532**, 130174 (2025).
- ³⁸P. Sarkar, R. Chattopadhyay, and J. K. Bhattacharjee, Physical Review E **110**, 034207 (2024).
- ³⁹B. Sundaram and P. W. Milonni, Physical Review E **51**, 1971 (1995).
- ⁴⁰D. Brizuela, Physical Review D **90**, 085027 (2014).
- ⁴¹L. C. Baird, American Journal of Physics **40**, 327 (1972).
- ⁴²D. F. Styer, American Journal of Physics **58**, 742 (1990).
- ⁴³L. E. Ballentine and S. M. McRae, Physical Review A **58**, 1799 (1998).
- ⁴⁴D. Brizuela, Physical Review D **90**, 125018 (2014).
- ⁴⁵L. Jia, H. Xing, and L. Fu, Physical Review A **106**, 022814 (2022).
- ⁴⁶A. Marais, B. Adams, A. K. Ringsmuth, M. Ferretti, J. M. Gruber, R. Hendrikx, M. Schuld, S. L. Smith, I. Sinayskiy, T. P. J. Krüger, et al., Journal of the Royal Society Interface **15**, 1 (2018).
- ⁴⁷J. Izaac and J. Wang, *Computational Quantum Mechanics*, Undergraduate Lecture Notes in Physics (Springer, Cham, Switzerland / Netherlands, 2018), ISBN 978-3-319-99929-6.